Tumor-Driven Paracrine Platelet-Derived Growth Factor Receptor α Signaling Is a Key Determinant of Stromal Cell Recruitment in a Model of Human Lung Carcinoma

Max L. Tejada,[1] Lanlan Yu,[1] Jianying Dong,[1] Kenneth Jung,[3] Gloria Meng,[4] Franklin V. Peale,[2] Gretchen D. Frantz,[2] Linda Hall,[2] XiaoHuan Liang,[1] Hans-Peter Gerber,[1] and Napoleone Ferrara[1]

Abstract Activated fibroblasts are thought to play important roles in the progression of many solid tumors, but little is known about the mechanisms responsible for the recruitment of fibroblasts in tumors. Using several methods, we identified platelet-derived growth factor A (PDGFA) as the major fibroblast chemoattractant and mitogen from conditioned medium generated by the Calu-6 lung carcinoma cell line. In addition, we showed that Calu-6 tumors express significant levels of PDGFC, and that the levels of expression of these two PDGFRα ligands correlate strongly with the degree of stromal fibroblast infiltration into the tumor mass. The most intense expression of PDGFRα was observed in fibroblasts in the tumor outer rim. We subsequently showed that disrupting PDGFRα-mediated signaling results in significant inhibition of tumor growth *in vivo*. Furthermore, analysis of a compendium of microarray data revealed significant expression of PDGFA, PDGFC, and PDGFRα in human lung tumors. We propose that therapies targeting this stromal cell type may be effective in treating certain types of solid tumors.

It has become apparent that the microenvironment in which tumor cells develop profoundly influences many steps of tumor progression. The tumor microenvironment consists of a stroma, which is composed of immune and inflammatory cells, endothelial cells and fibroblasts, a variety of growth factors and cytokines, and an insoluble extracellular matrix. In various experimental tumor models, each of the stromal cell types has been shown to influence the efficiency of tumor formation, the rate of tumor growth, the extent of invasiveness, and the ability of the tumor cells to metastasize (1–3).

Much attention has been focused on the role of endothelial cells in tumor angiogenesis; however, there is accumulating evidence that in many solid tumor types, the influence of the microenvironment is mediated in large part by paracrine signaling between the tumor epithelium and neighboring stromal fibroblasts (4). Fibroblasts are the major constituent of the stroma in many solid tumors, and in some cases, the fibroblast stroma comprises >90% of the tumor mass. These tumor-associated fibroblasts often exist in a constitutively activated state and often exhibit biological markers consistent with those found at the sites of normal wound healing (3).

In the normal wound repair process, fibroblasts are recruited from the surrounding tissue. However, cancer cells are capable of recruiting fibroblasts from the surrounding environment and inducing their activation to the myofibroblast phenotype directly (3). In addition to their presence in the tumor mass, myofibroblasts are often found at the invasive fronts of a number of solid tumors, where they have been shown to affect the growth, invasion, and metastasis of the tumors through their increased synthesis of extracellular matrix components and the increased production of proteases, growth, and angiogenic factors (4).

The growth of solid tumors requires the formation of new blood vessels through angiogenesis, the sprouting of new blood vessels from preexisting ones, although more recent evidence indicates that recruitment of bone marrow–derived angiogenic cells contributes to the development of a neovascular supply (5, 6). Although a number of angiogenic factors have been identified, vascular endothelial growth factor A (VEGF-A) is probably the most ubiquitous, and much experimental evidence implicates this factor in the regulation of both physiologic and pathologic angiogenesis (7, 8). Administration of an anti-VEGF-A humanized monoclonal antibody (mAb; bevacizumab) in combination with chemotherapy results in increased survival relative to chemotherapy alone in patients with previously untreated metastatic colorectal cancer (9). In several experimental systems, inactivation of the *VEGF-A* gene indicates that tumor-derived VEGF is important for tumor angiogenesis and growth (10, 11). However, other studies have detected significant levels of VEGF in the stromal compartment, suggesting a significant role for stromal fibroblast-derived VEGF (12, 13).

Members of the platelet-derived growth factor (PDGF) family have been shown to be potent mitogens and chemoattractants

Authors' Affiliations: Departments of [1]Molecular Oncology, [2]Pathology, [3]Bioinformatics and Assay, and [4]Automation Technology, Genentech, Inc., South San Francisco, California

Received 8/12/05; revised 12/22/05; accepted 2/17/06.

The costs of publication of this article were defrayed in part by the payment of page charges. This article must therefore be hereby marked *advertisement* in accordance with 18 U.S.C. Section 1734 solely to indicate this fact.

Note: Supplementary data for this article are available at Clinical Cancer Research Online (http://clincancerres.aacrjournals.org/).

Requests for reprints: Napoleone Ferrara, Department of Molecular Oncology, Genentech, Inc., 1 DNA Way, South San Francisco, CA 94080. Phone: 650-225-2968; Fax: 650-225-6443; E-mail: nf@gene.com.

doi:10.1158/1078-0432.CCR-05-1770

for a wide variety of cell types of mesenchymal origin (14). In both human and mouse, the PDGF family consists of four members (PDGFA, PDGFB, PDGFC, and PDGFD), which exert their biological effects by binding to two receptor tyrosine kinases (PDGFRα and PDGFRβ). PDGFAA, PDGFAB, PDGFBB, and PDGFCC dimers bind to PDGFRα with high affinity, whereas PDGFBB and PDGFDD dimers bind PDGFRβ preferentially. PDGF signaling is critical for proper embryonic development, whereas in the adult, it plays a role in wound healing and in the control of interstitial fluid pressure (14).

Aberrant PDGF signaling is a hallmark of a number of solid tumors, and studies of breast, lung, and colon cancers have shown a tight correlation between deregulated paracrine PDGF signaling and cancer progression (15–17). Furthermore, in gliomas, fibrosarcomas, and osteosarcomas, coexpression of the PDGF ligands and their cognate receptors by the tumor cells leads to an autocrine mechanism that drives carcinogenesis (18–20). Unlike the other members of its family, PDGFAA exhibits a weak transforming activity, and thus far, most of the studies have focused on its role in embryonic development (21).

Many studies have focused upon the role of tumor-derived factors, such as PDGFB, basic fibroblast growth factor, and transforming growth factor β-1 in the induction of the myofibroblast phenotype and the angiogenic process (22–24). However, attempts to identify bona fide tumor-derived stromal fibroblast recruitment factors are rare, despite the fact that intuitively, this precedes fibroblast activation (25–27). In addition, using a dominant-negative strategy, Shao et al. showed that the expression of several PDGF family members was responsible for a desmoplastic response in mammary gland tumor xenografts (28).

Recently, using fibrosarcomas derived from *VEGF* null mouse embryonic fibroblasts, Dong et al. showed a crucial role for PDGFA in the recruitment of a stroma capable of mediating tumor angiogenesis in the absence of tumor-derived VEGF (29). However, the relevance of these findings to human tumors remained unknown. To investigate the mechanisms of stromal recruitment in a model of human lung carcinoma, we used the Calu-6 cell line that is characterized by its ability to elicit a significant host stromal response *in vivo*. Using chromatographic and immunologic methods, we identified PDGFAA as the major chemotactic and mitogenic activity whose levels correlate positively with the Calu-6 tumor's ability to elicit a significant stromal response *in vivo*. Adenoviral delivery of selective antagonists of PDGF signaling showed that disrupting PDGFRα signaling inhibits tumor growth *in vivo*. To validate these findings, we analyzed the GeneExpress compendium of microarray data and confirmed the significant expression of PDGFA and PDGFC as well as their cognate receptor PDGFRα in human lung tumor samples. Thus, inhibition of signaling through PDGFRα may prove to be an effective method of affecting the growth and development of certain human solid tumors by targeting recruitment of the stromal fibroblasts.

Materials and Methods

Cell lines. The human lung carcinoma cell line Calu-6 cell line and the mouse fibroblast cell line NIH3T3 (American Type Culture Collection, Manassas, VA) were cultured routinely in growth medium [Ham's F12 50%, low-glucose DMEM 50% supplemented with 10% v/v fetal bovine serum, 1% v/v penicillin/streptomycin, 2 mmol/L L-glutamine, and 1 μg/mL Fungizone (Invitrogen, Carlsbad, CA)]. Cells were incubated at 37°C in an atmosphere of 95% air/5% CO_2. The human embryonic kidney 293 cell line (American Type Culture Collection), used to generate the adenovirus used in these experiments, was typically grown using high-glucose DMEM supplemented with 10% v/v fetal bovine serum, 1% v/v penicillin/streptomycin, 2 mmol/L L-glutamine, and 1 μg/mL Fungizone (Invitrogen).

Generation and fractionation of conditioned medium. Calu-6 cells were allowed to grow to confluency in the presence of growth medium on gelatin-coated 500-cm^2 dishes. The medium was then replaced with serum-free DMEM/Ham's F12 medium, and the cells were incubated for an additional 72 hours, at which time the media (total of 6 liters) was harvested and concentrated 5-fold using a Filtron Ultrasette tangential flow device with 10K membrane (Filtron Technology Corp., Northborough, MA). All fractionation procedures described were done using an AKTA Explorer chromatography system (GE Healthcare Bio-Sciences Corp., Piscataway, NJ).

Cation-exchange column chromatography. The concentrated medium was dialyzed against 25 mmol/L sodium phosphate (pH 6) and applied on a 5-mL HiTrapS Sepharose column (Amersham Pharmacia Biotech), which had been equilibrated with the same buffer. After a low salt wash, the column was eluted with 1 mol/L NaCl.

Size exclusion column chromatography. Bioactive 1 mol/L NaCl fractions generated using cation-exchange chromatography were pooled, and 5-mL aliquots were loaded onto a TSK3000 column (21.5 × 30 cm; Tosoh Biosep LC, Montgomeryville, PA) that had been equilibrated in 20 mmol/L Tris (pH 7.5), 2 mol/L NaCl, and 0.02% Tween 20. The flow rate was 3 mL/min, 3-mL fractions were collected, and aliquots were tested for bioactivity.

Reverse-phase column chromatography. Bioactive fractions generated using size exclusion chromatography were pooled, diluted 5-fold in water containing 0.1% trifluoroacetic acid and loaded onto a C4 4000A column (4.6 × 100 mm). The column was eluted using a linear gradient of 15% to 50% acetonitrile (120 minutes) in 0.1% (v/v) trifluoroacetic acid at the flow rate of 0.6 mL/min. Fractions of 0.6 mL were collected and tested for bioactivity.

Proliferation assays. NIH3T3 cells were seeded on 96-well plates (BD Biosciences, Bedford, MA) at a density of 3,000 in a 100 μL final volume. Following overnight incubation, the medium was replaced with starvation media (0.1% w/v bovine serum albumin in DMEM/Ham's F12 medium) supplemented with 2 to 10 μL of each fraction to be tested, to a final volume of 100 μL. Following overnight incubation, 1 μCi of ^{3}H-methyl thymidine was added to each well, and the cells incubated for 6 hours before harvesting. Cellular DNA was harvested using a Filtermate 196 Harvester (Perkin Elmer, Wellesley, MA) and Unifilter-96, GF/C plates (part no. 6005174; Perkin-Elmer, Wellesley, MA). Incorporation of ^{3}H-methyl thymidine was detected using a TopCount Microplate Scintillation Counter (Packard Bioscience). The data were plotted as total cpm of incorporated over the fraction number. Inhibition assays were done as described above, except that soluble PDGFRα or PDGFRβ was included in the assay mixtures at a final concentration of 1 μg/mL (>30 nmol/L). The samples were then processed as described. To rule out the possibility that the effects of the soluble PDGFRs were nonspecific, we tested the ability of such soluble receptors to inhibit the effects of a variety of unrelated growth factors, including basic fibroblast growth factor, epidermal growth factor, hepatocyte growth factor, PDGFA, and PDGFB, on fibroblast proliferation and found no inhibitory effects at the concentrations used to affect the bioactivity present in the Calu-6 conditioned medium.

To assess Calu-6 proliferation, the Calu-6 cells were seeded in a final volume of 1 mL in growth medium at a density of 3,000 per well in a 24-well plate (BD Biosciences, Bedford, MA). Following overnight incubation, the medium was replaced with assay medium (0.5% v/v fetal bovine serum in DMEM/Ham's F12 medium) that included either soluble PDGFRα or PDGFRβ at concentrations of 1 or 5 μg/mL (30 and 150 nmol/L, respectively). As controls, the cells were grown in assay media supplemented with basic fibroblast growth factor, epidermal

growth factor, PDGFAA, or PDGFBB at final concentrations of 20 μg/mL or in the presence of complete 50:50 media (10% fetal bovine serum). Following a 5-day incubation, the cells were trypsinized and counted using a Coulter Counter (Beckman Coulter, Miami, FL). The results are presented as total cell numbers over treatment.

Migration assays. A modified Boyden chamber migration assay was done using 24 transwell Fluoroblok migration plates (HTS Fluoroblock Multiwell Insert System, BD Clontech, Mountain View, CA). The plates (8 μm pore size) were precoated with 0.1% w/v gelatin. A 700-μL final volume of starving media incorporating 10 to 20 μL samples of the fractions to be tested were placed on the lower chamber of the chemotaxis plates. Alternatively, a negative buffer-only control and controls containing either PDGFAA or PDGFBB at a final concentration of 20 ng/mL was used. Subsequently, 40,000 NIH3T3 cells were plated in a final volume of 200 μL onto the upper chamber. Following overnight incubation at 37°C in an atmosphere of 95% air/5% CO_2, the medium in the both upper and lower chambers was aspirated, and the cells were fixed in cold methanol for 20 minutes at 4°C. The methanol was removed, and the plates were dried at room temperature before staining in a final concentration of 1 mmol/L YoPro-1 (Invitrogen, Eugene, OR) in PBS. Migration was assessed fluorimetrically using a CytoFluor Multiwell Plate Reader and CytoFluor Software (Series 4000; Applied Biosystems, Foster City, CA). Results are presented as relative fluorescence units over fraction number. Inhibition assays were done as described above, except that soluble PDGFRα or PDGFRβ was included in the assay mixtures at a final concentration of 1 μg/mL (>30 nmol/L). The samples were then treated as described.

ELISA. Fractions were assayed for human PDGFAA, PDGFAB, and PDGFBB using the Quantikine (DAA00, DHD00B, and DB00; R&D Systems, Minneapolis, MN). Tumor lysates were assayed using a human VEGF-specific ELISA (DVE00; R&D Systems). The concentration of murine VEGF was determined using an ELISA developed at Genentech (South San Francisco, CA). Briefly, goat anti-mouse VEGF antibody (R&D Systems) was diluted to 1 μg/mL in coating buffer [50 mmol/L sodium carbonate (pH 9.6)] and used to coat a Maxisorp 96-well plate (100 μL/well; Nunc, Rochester, NY). Following overnight incubation at 4°C, the plate was washed thrice (0.05% v/v Tween 20 in PBS), 150 μL blocking buffer [0.05% w/v bovine serum albumin, 10 ppm Proclin 300 (Sigma-Aldricht, St. Louis, MO) in PBS] added and incubated for 1 hour at room temperature. The plate was washed six times, and murine VEGF standards (3.2-500 pg/mL) and the samples were diluted using assay buffer [0.05% w/v bovine serum albumin, 0.2% w/v bovine γ-globulin, 0.25% w/v CHAPS, 5 mmol/L EDTA, 0.35 mol/L NaCl, 0.05% v/v Tween 20 in PBS (pH 7.4)] were added (100 μL/well). Following a 2-hour incubation at room temperature, the plate was washed six times, and a biotinylated goat anti-mouse VEGF antibody was added (100 μL/well). After a 1-hour incubation at room temperature, the plates were washed six times, and streptavidin-horseradish peroxidase (GE Healthcare Bio-Sciences, Piscataway, NJ), made in assay buffer, was added (100 μL/well). The plate was incubated for 1 hour at room temperature and washed six times, and 100 μL of biotinyltyramide from the ELAST Amplification kit (Perkin-Elmer Life Sciences, Inc., Wellesley, MA) was added to each well. Following a 15-minute incubation at room temperature, the plate was washed six times and incubated with streptavidin-horseradish peroxidase (100 μL/well) for 30 minutes and washed six times, and 100 μL of TMB (Kirkegaard and Perry Laboratories, Gaithersburg, MD) was added to each well. The color was allowed to develop for 2 to 3 minutes at room temperature and stopped by adding 100 μL of 1 mol/L H_3PO_4 to each well. The absorbance was read at 450/650 nm using a SpectraMax 250 microplate reader (Molecular Devices Corp., Sunnyvale, CA).

Western blotting for fibronectin. Fractions generated from size exclusion chromatography of Calu-6 conditioned medium were concentrated 4-fold using Microcon YM-3 columns (Millipore Corp., Billerica, MA) and separated using a 4% to 20% gradient SDS-PAGE (Invitrogen). Following electrophoretic transfer to a polyvinylidene difluoride membrane, the blot was probed overnight using a mAb against human-fibronectin (MAB1934, Chemicon, Temecula, CA) diluted to a concentration of 5 μg/mL in blocking buffer (PBST, 0.1% v/v Tween 20 in PBS and 5% w/v skim milk powder). The blot was washed thrice using wash buffer (0.2% w/v skim milk powder in PBST) and probed with a horseradish peroxidase–conjugated goat anti-mouse IgG (Pierce Chemical, Rockford, IL) diluted 1:20,000 in blocking buffer. Following three washes, the blot was developed using the enhanced chemiluminescence plus Western Blotting Detection System (RPM2132; GE Healthcare Bio-Sciences, Piscataway, NJ).

Quantitative reverse transcription-PCR analysis. Primers specific for human *PDGF* chains A, B, C, D and *glyceraldehyde-3-phosphate dehydrogenase* or *RPL19*; murine *VEGF-A* and *glyceraldehyde-3-phosphate dehydrogenase*; and an oligonucleotide probe labeled with a reported fluorescent dye (FAM) at the 5′ end and a quencher fluorescent dye (TAMRA) at the 3′ end were designed using the ABI PRISM PrimerExpress version 1.5 software (PE Applied Biosystems, Foster City, CA). The quantitative reverse transcription-PCR (RT-PCR) primer sequences are provided in Table 1. Total RNA was isolated from xenografted tumor samples or monolayer by homogenization in the presence of Tri Reagent and BCP phase separation reagent (Molecular Research Center, Cincinnati, OH) according to the manufacturer's protocol. The RNA was subsequently cleaned using the RNeasy Protect Midi kit (Qiagen, Valencia, CA). Total RNA (50 ng) was added to a 50 μL RT-PCR reaction mixture according to the manufacturer's protocol (Roche Molecular Systems, Pleasanton, CA). The thermal cycling conditions included one cycle at 48°C for 30 minutes, one cycle at 95°C for 10 minutes, 40 cycles at 95°C for 15 seconds, annealing at 60°C for 1 minute, and a final hold at 25°C for 2 minutes. These reactions were done in MicroAmp Optical 96-well reaction plates and run on an ABI PRISM 7700 Sequence Detector (PE Applied Biosystems). Standard curves for the expression of each gene were generated by serial dilution of a standard preparation of total RNA from the human glioma cell line G55, or normal human lung (BD Clontech).

Analysis of normal and tumor human lung samples. The expression of members of the PDGF family were analyzed in GeneExpress (Genelogic, Gaithersburg, MD), a compendium of microarray gene expression data from thousands of clinical samples. Using this database, 138 normal human lung and 159 human lung tumor samples were examined using probes specific for each member of the PDGF family. Signal intensity (arbitrary units) was computed using Affymetrix MAS 5 software (Affymetrix, Inc., Santa Clara, CA). Normal samples are shown in green above the respective lines for each PDGF, whereas tumor samples are shown in red; *t* statistics and their corresponding two-tailed *P*s were calculated using the R program for statistical computing (http://www.r-project.org), assuming unequal variance in the normal and tumor groups. $P < 0.0001$ was considered statistically significant.

Generation of adenoviral constructs. cDNA encoding the *β-galactosidase* gene, a region encoding the first three immunoglobulin-like domains of murine VEGFR1 fused to the Fc portion of murine IgG1 [mFlt(1-3)-IgG], and the extracellular domain that includes the first three immunoglobulin domains of either PDGFRα or PDGFRβ fused to the Fc portion of human IgG1 (PDGFRα-IgG and PDGFRβ-IgG) were cloned into the cytomegalovirus shuttle vector using *Not*I and *Hin*dIII sites, and recombinant virus was produced using the AdEasy system according to the manufacturer's directions (Stratagene, La Jolla, CA). Virus was purified by using the Megakit from Virapur (BD Clontech) and titered by conventional methods.

Mouse xenograft experiments. Briefly, Calu-6 cells suspended at a concentration of 5×10^6 per mL Matrigel were injected s.c. into the dorsal flank region of beige nude XID mice (Harlan Sprague-Dawley, Indianapolis, IN). Five days after tumor cell inoculation, when the xenografts were established and had reached a volume of 50 to 100 mm^3, i.p. treatment with mAb A.4.6.1 (30) was initiated, at a dose of 10 mg/kg. Thereafter, the mice were treated twice weekly. mFlt(1-3)-IgG, also designated as mFlt-IgG, was administered i.p. every day at a dose of 25mg/kg. Tumor volumes were calculated every second day using the ellipsoid volume formulas ($6 \times L \times W \times H$, where L = length, W =

Table 1. Quantitative RT-PCR primer sequences used in these experiments

Primer	Sequence	Orientation	Gene
187486	5-CCTTTCCTGGGACATGGA-3	Forward	*PDGFA*
187487	5-GCACACTGGCAATAAAGCA-3	Reverse	*PDGFA*
187488	5-TACATGGCGTGTTACATTCCTGAACCTACT-3	Probe	*PDGFA*
166036	5-CGATCCGCTCCTTTGATGAT-3	Forward	*PDGFB*
166037	5-TCCAACTCGGCCCCATCT-3	Reverse	*PDGFB*
166038	5-CTGCACGGAGACCCCGGAGAGG-3	Probe	*PDGFB*
166039	5-GCCTCTTCGGGCTTCTCC-3	Forward	*PDGFC*
166040	5-TTACTACTCAGGTTGGATTCCGC-3	Reverse	*PDGFC*
166041	5-CTGACATCTGCCCTGGCCGGC-3	Probe	*PDGFC*
166042	5-CAGTAACGGATCCCACTCTGATT-3	Forward	*PDGFD*
166043	5-TTGAGCAGATCTTCCACTGTATCAA-3	Reverse	*PDGFD*
166044	5-CGGATGCTCTGGACAAAAAAATTGCAGAA-3	Probe	*PDGFD*
124570	5-ATGAAGCCCTGGAGTGCGT-3	Forward	*VEGF*
124571	5-AGGTTTGATCCGCATGATCTG-3	Reverse	*VEGF*
124572	5-CCCACGTCAGAGAGCAACATCACCAT-3	Probe	*VEGF*
201073	5-TGGGCTACACTGAGCACCAG-3	Forward	*GAPDH*
201074	5-CAGCGTCAAAGGTGGAGGAG-3	Reverse	*GAPDH*
201075	5-TCTCCTCTGACTTCAACAGCGACACCC-3	Probe	*GAPDH*
209729	5-AGCGGATTCTCATGGAACA-3	Forward	*RPL19*
209730	5-CTGGTCAGCCAGGAGCTT-3	Reverse	*RPL19*
209731	5-TCCACAAGCTGAAGGCAGACAAGG-3	Probe	*RPL19*

width, and H = height; ref. 31). For statistical analysis of differences between groups, a one-way ANOVA followed by a Tukey HSD pairwise analysis was done using JMP software (SAS Institute, Inc., Cary, NC). $P < 0.001$ was considered significant.

Calu-6 cells were resuspended in Matrigel (BD Clontech) at a concentration of 1×10^8 cells/mL and injected (100 μL/mouse) s.c. into the dorsal flank regions of Beige XID mice (Harlan Sprague-Dawley) using a 28-gauge needle and 0.5-mL tuberculin syringe. Following a 24-hour incubation, the mice were separated into groups of six, and the tumor volumes were determined by measurement along their length × width × height using vernier calipers (32). The mice were then injected i.t. with 1×10^9 plaque-forming units of each adenovirus in 100 μL volume. Treatment was done once per week for a period of 4 weeks, at which time the tumors were measured, excised, and weighed, and portions were snap-frozen in liquid nitrogen for RNA extraction or fixed in 10% v/v formalin for subsequent analysis. Data are presented as the mean ± SE of six mice per group. For statistical analysis of differences between groups, a one-way ANOVA followed by a Tukey HSD pairwise analysis was done using JMP software (SAS Institute). $P < 0.001$ was considered significant.

Generation of tumor lysates. Tumor lysates were prepared by homogenization in cold modified radioimmunoprecipitation assay buffer [50 mmol/L Tris-HCl (pH 7.2), 100 mmol/L sodium chloride, 1 mmol/L EDTA, 1 mmol/L phenylmethylsulfonyl fluoride, 1% v/v Triton X-100, 0.5% w/v sodium deoxycholic acid, 0.1% w/v SDS, 1 mmol/L sodium orthovanadate, 1 mmol/L sodium fluoride] supplemented with 1 Complete protease inhibitor cocktail tablet (Roche Diagnostics, Indianapolis, IN) per 50 mL of buffer. Tissue and cell debris was removed by centrifugation. Protein concentration was determined with a modified bicinchoninic acid protein assay (Pierce Chemical) as per the manufacturer's instructions.

In situ *analyses of xenografted tumor samples.* All tissues were fixed in 10% (v/v) formalin and paraffin embedded. Sections 5-μm thick were deparaffinized, deproteinated in 4 μg/mL of proteinase K for 30 minutes at 37°C, and further processed for *in situ* hybridization as previously described (33, 34). ^{33}P-UTP labeled sense and antisense probes were hybridized to the sections at 55°C overnight. Unhybridized probe was removed by incubation in 20 μg/mL RNase A for 30 minutes at 37°C followed by a high stringency wash at 55°C in 0.1 × SSC for 2 hours and dehydration through graded ethanol. The slides were dipped in NBT2 nuclear track emulsion (Eastman Kodak, Rochester, NY), exposed in sealed plastic slide boxes containing desiccant for 4 to 6 weeks at 4°C, developed, and counterstained with H&E. The following probe templates were PCR amplified using the primers described below. Upper primers and lower primers for murine *VEGF* exon 3, murine *PDGFA*, and murine *PDGFB* had 27 nucleotide extensions appended to the 5′ ends encoding T7 RNA polymerase and T3 RNA polymerase promoters, respectively, for generation of sense and antisense transcripts. *mVEGF* exon 3 probe: 193 nucleotides corresponding to nucleotides 202-394 of NM_009505, upper primer, 5′-TGATCAAGTTCATGGACGTCTACC-3′ and lower primer, 5′-ATGGTGATGTTGCTCTCTGACG-3′. Murine *PDGFA* probe: 571 nucleotides corresponding to nucleotides 192-762 of NM_008808, upper primer, 5′-TGGGCTTGCCTGCTGCTCCT-3′ and lower primer, 5′-CTGTCTCCTCCTCCCGATGGTCT-3′. Murine *PDGFB* probe: 653 nucleotides corresponding to nucleotides 1082-1734 of NM_011057, upper primer, 5′-CACTCCATCCGCTCCTTTGA-3′ and lower primer, 5′-AAATAACCCTGCCCACACTCTTG-3′. Two templates were generated for murine *PDGFRα*, *PDGFRβ*, human *PDGFA*, and human *PDGFB* with T7 RNA polymerase promoters appended to the 5′ end of either the upper primer for sense transcripts or the lower primer for antisense transcripts. *mPDGFRα* probe: length 799 nucleotides corresponding to nucleotides 268-1066 of NM_011058, upper primer, 5′-TTACCCTCTATCCTCCCAAACGA-3′ and lower primer, 5′-GGGCAGCACATTCATACTCTCC-3′. *mPDGFRβ* probe: 742 nucleotides corresponding to nucleotides 574-1315 of NM_008809, upper primer, 5′-ATTCCGTGCCGAGTGACAGACCC-3′ and lower primer, 5′-AGTAGCCCGCTTCTGACACCTT-3′. Human *PDGFA* probe: 578 nucleotides corresponding to nucleotides 844-1421 of NM_002607, upper primer, 5′-GACCTTGGCTTGCCTGCTGCTCC-3′ and lower primer, 5′-TTCCCGTGTCCTCTTCCCGATAA-3′. Human *PDGFB* probe: 621 nucleotides corresponding to nucleotides 1037-1657 of NM_002608, upper primer, 5′-GGCGCTCTTCCTGTCTCTCTGCT-3′ and lower primer, 5′-GTCCGAATGGTCACCCGAGTTTG-3′.

Immunohistochemical analyses of xenografted tumor samples. Tumors were fixed in neutral-buffered formalin for 24 hours before paraffin embedding. H&E staining and immunohistochemistry were done as described previously (33). Immunohistochemical staining was done using the antigen retrieval systems and appropriate antibodies listed in Table 2. Each was detected sequentially using the appropriate biotinylated secondary antibody, Vectastain Avidin-Biotin Complex Peroxidase Elite and Vectastain Elite, or streptavidin-alkaline phosphatase (Vector Laboratories, Burlingame, CA). Reaction product was generated using metal-enhanced 3,3′-diaminobenzidine (Pierce Chemical) or Vector Blue (Vector Laboratories) as appropriate. Sections were lightly counterstained with hematoxylin, dehydrated, and coverslipped.

Results

Stromal cell recruitment correlates with the resistance to antihuman VEGF therapy in a xenograft model. To examine the influence of the stroma on the response of these tumors to anti-VEGF therapy, we made use of a human tumor cell line, Calu-6, which is characterized by its ability to induce a strong host stromal response *in vivo*. In several experiments, Calu-6 tumor growth was minimally inhibited by treatment with mAb A4.6.1, an antibody recognizing human VEGF (30). Figure 1A illustrates a representative experiment in which only 5% inhibition was achieved. However, treatment of these tumors with mFlt(1-3)-IgG, a soluble form of VEGFR1 that binds and sequesters both tumor- and host-derived VEGF, resulted in growth inhibition of >90% (35). In contrast, the A673 rhabdomyosarcoma cell line, which results in a more modest stromal recruitment *in vivo* relative to Calu-6 cells, was shown in previous studies to be inhibited ≥80% by treatment with mAb A4.6.1 (36).

To assess the relative contributions of tumor and stroma to the resistance of Calu-6 tumors to treatment with mAb A4.6.1, the levels of tumor- and host-derived VEGF were examined. In the Calu-6 tumors, both the tumor and stromal cells produce nearly equivalent levels of VEGF [52.2% and 47.8 ± 7.1% (SE), respectively]. In contrast, a majority of the VEGF detected in the A673 tumors is generated by the tumor cells [97.6 ± 0.7% (SE)].

Next, the tumors were examined histologically to assess the correlation between the level of stromal-derived VEGF and the degree of stromal cell incorporation into the tumor. Although the Calu-6 tumor cells were surrounded by spindle-like stromal cells that displayed fibroblast morphology and smooth muscle actin immunoreactivity (Fig. 1B), the A673 tumors almost completely comprised sheets of tumor cells with little stromal infiltration (Fig. 1C).

Calu-6 cells secrete a potent fibroblast bioactive factor. The extensive incorporation of stromal fibroblasts into the Calu-6 tumor mass (Fig. 1B) suggested that these tumor cells could be a source of stromal mitogens and chemoattractants. Therefore, Calu-6 conditioned medium was generated and subjected to column chromatography. Both mitogenic and chemotactic activities were monitored using the NIH3T3 fibroblast cell line, which was used as a stromal fibroblast cell model because it has proven to be a more robust cell type than primary stromal cell cultures (data not shown). This was important given the harsh nature of some of the buffers used in the purification protocol. Calu-6 conditioned medium was subjected to cation-exchange chromatography, and fractions 4 to 8 were found to contain potent mitogenic and chemotactic activities (Fig. 2A and B, respectively). These fractions were pooled and subjected to size exclusion chromatography. Fractions 30 to 32, corresponding to an M_r of 20 to 45 kDa, contained a potent mitogenic (Fig. 2C) and chemotactic (Fig. 2D) activity. These fractions were pooled and purified further by reverse-phase chromatography. Again, prominent mitogenic and chemotactic activities (Fig. 2E and F, respectively) coeluted in fractions 15 to 22, which corresponded to 25% to 35% acetonitrile.

Calu-6 cells express significant levels of PDGFA and PDGFC. Previous studies aimed at characterizing novel fibroblast chemoattractants identified fibronectin as the major bioactive factor (25–27). Therefore, a number of size-excluded fractions ranging in size from 15 to 670 kDa were examined for the presence of fibronectin by Western blotting. Fibronectin is present in the fractions of molecular weight of >158 kDa (Fig. 3A), which represent a minor portion of the total chemotactic activity in Calu-6 conditioned medium and were subsequently excluded from further purification. A candidate approach was then taken to try to identify the factors present in the major peaks of bioactivity. Because members of the PDGF family are the most potent fibroblast mitogens and chemoattractants, the fractions were initially tested for PDGFBB or PDGFAB, and their levels were determined to be below the limits of detection by ELISA (<31.25 pg/mL). In contrast, significant amounts of PDGFAA (>30 ng/mL per fraction) were found to coelute with the major peak of activity in the size-excluded fractions (Fig. 3B). The bioactive fractions generated

Table 2. Summary of antibodies and reagents

Antibody	Source	Primary antibody	Primary antibody (μg/mL)	Antigen retrieval	Secondary antibody	Secondary antibody (μg/mL)
PDGFRα	R&D Systems	Goat polyclonal AF1062	1	Target, High pH	Rabbit anti-goat, biotinylated	7.5
PDGFRβ	R&D Systems	Goat polyclonal AF1062	1	Trilogy	Rabbit anti-goat, biotinylated	7.5
αSMA	DAKO, Indianapolis, IN	Mouse monoclonal 1A4	0.1	None	Goat anti-mouse, biotinylated	5
MECA-32 (PVLAP endothelial antigen)	PharMingen/ BD Biosciences	Rat monoclonal	2	Target	Rabbit anti-rat biotinylated	2.5

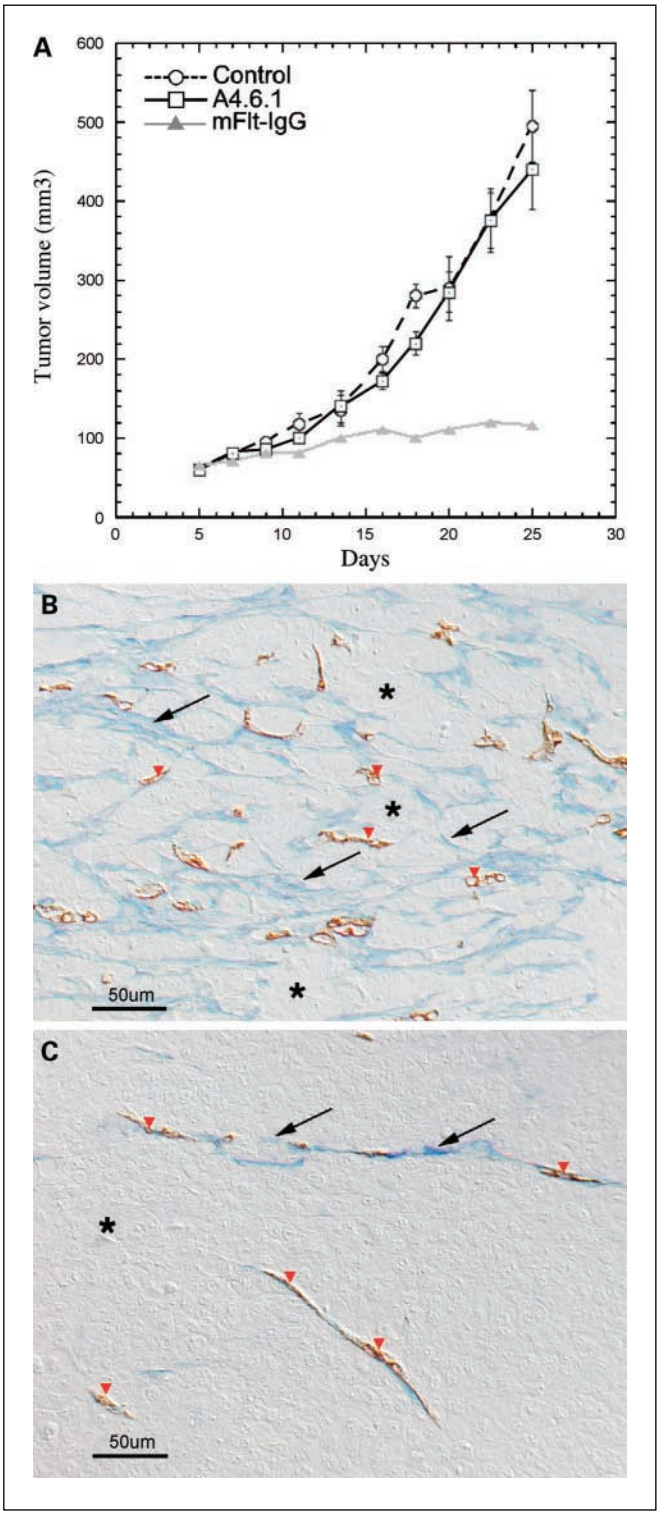

Fig. 1. Response of Calu-6 tumors to anti-VEGF therapy. *A,* growth curves of control untreated Calu-6 lung carcinoma – derived xenografted tumors, tumors treated with mAb A4.6.1, or tumors treated with mFlt-IgG. Tumor volume (mm^3) over time in days. *B* and *C,* sections of the Calu-6 or A673 tumors were stained with antibodies to the endothelial cell marker PVLAP (*triangles*) and αSMA (*arrows*). *, tumor cells. Images were taken using differential interference contrast microscopy to visualize the tumor (*asterisk*) and stromal (*arrows*) constituents. *B,* Calu-6 tumors exhibit significant infiltration by stromal cells (*arrows*) and substantial acellular matrix. Anti-PLVAP staining was used to highlight the vasculature (*triangles*). *C,* A673 tumors almost completely comprised primitive skeletal muscle cells (*asterisk*) with minimal stromal infiltration.

by cation-exchange or reverse-phase column chromatography were also tested and found to contain considerable amounts of PDGFAA (data not shown).

We also tested for the presence of PDGFAA and PDGFBB in the conditioned medium generated from a variety of human cancer cell lines whose respective tumors are associated with substantial amounts of stroma (Table 3). The results show considerable expression of PDGFAA by these tumor cell lines. In contrast, PDGFBB was undetectable. Because there is a paucity of effective antibody reagents to test for the presence of either PDGFCC or PDGFDD, we used quantitative RT-PCR to assess the levels of the various PDGF family members in RNA isolated from Calu-6 cells using human PDGF-specific primers. Calu-6 cells express considerable levels of PDGFA and C, whereas PDGFB and PDGFD are virtually undetectable (Fig. 3C).

To assess the physiologic relevance of the results derived using the Calu-6 tumor model, we examined RNA isolated from tumors derived from a human pancreatic adenocarcinoma cell line HPAC, which is associated with a significant stromal response *in vivo* (37). Similarly to the Calu-6 tumors, HPAC tumors expressed significant levels of PDGFA and PDGFC, whereas the levels of PDGFB or PDGFD were barely detectable (Fig. 3D). ELISA done on the conditioned medium of this cell line indicated the presence of PDGFAA (0.608 ng/mL) at levels that were comparable with the levels detected in the Calu-6 conditioned medium (0.893 ng/mL). In contrast, A673 conditioned medium contains little PDGFAA (0.062 ng/mL). In all conditioned media, PDGFBB was undetectable (Table 3).

We also assessed the relative expression of each human PDGF in the Calu-6 and A673 tumors using quantitative RT-PCR. The results show significant expression of PDGFA and PDGFC by the Calu-6 tumors in contrast to the considerably lower levels detected in the A673 tumors. In both tumors, the levels of PDGFB were significantly lower, whereas the levels of PDGFD were barely detectable (Fig. 3E). ELISA was used to confirm the relative levels of PDGFAA and PDGFBB in Calu-6 tumor lysates. Although Calu-6 tumors contain significant levels of PDGFAA [267 ± 55 pg/mg total protein (SE)], the levels of PDGFBB are ≈3-fold lower [93.7 ± 24.9 pg/mg total protein (SE)]. Similar results were obtained in an independent experiment (data not shown).

To complement these studies, we analyzed the expression of the PDGFs and their cognate receptors using GeneExpress, a compendium of microarray gene expression data containing thousands of clinical samples. This analysis, which included 138 normal samples and 159 tumor samples, showed considerable PDGFA expression in the normal lung and the tumor samples. However, a subset of lung tumor samples (20 of 159), classified predominantly as adenocarcinomas, contained significantly higher levels of PDGFA (Fig. 3F). Interestingly, the overall levels of PDGFC were found to be higher in the tumor samples compared with the normal samples (mean signal intensities of 1,486 and 1,174 arbitrary units, respectively; $P < 0.0001$). In contrast, both PDGFB and PDGFD are expressed at lower levels overall, and no differences in expression were found in the normal compared with the tumor samples. The considerable expression of both PDGFRα and PDGFRβ detected in both normal and tumor samples coupled with the predominant expression of PDGFA and C suggests that this axis of PDGF signaling may be an important part in the development of lung cancer.

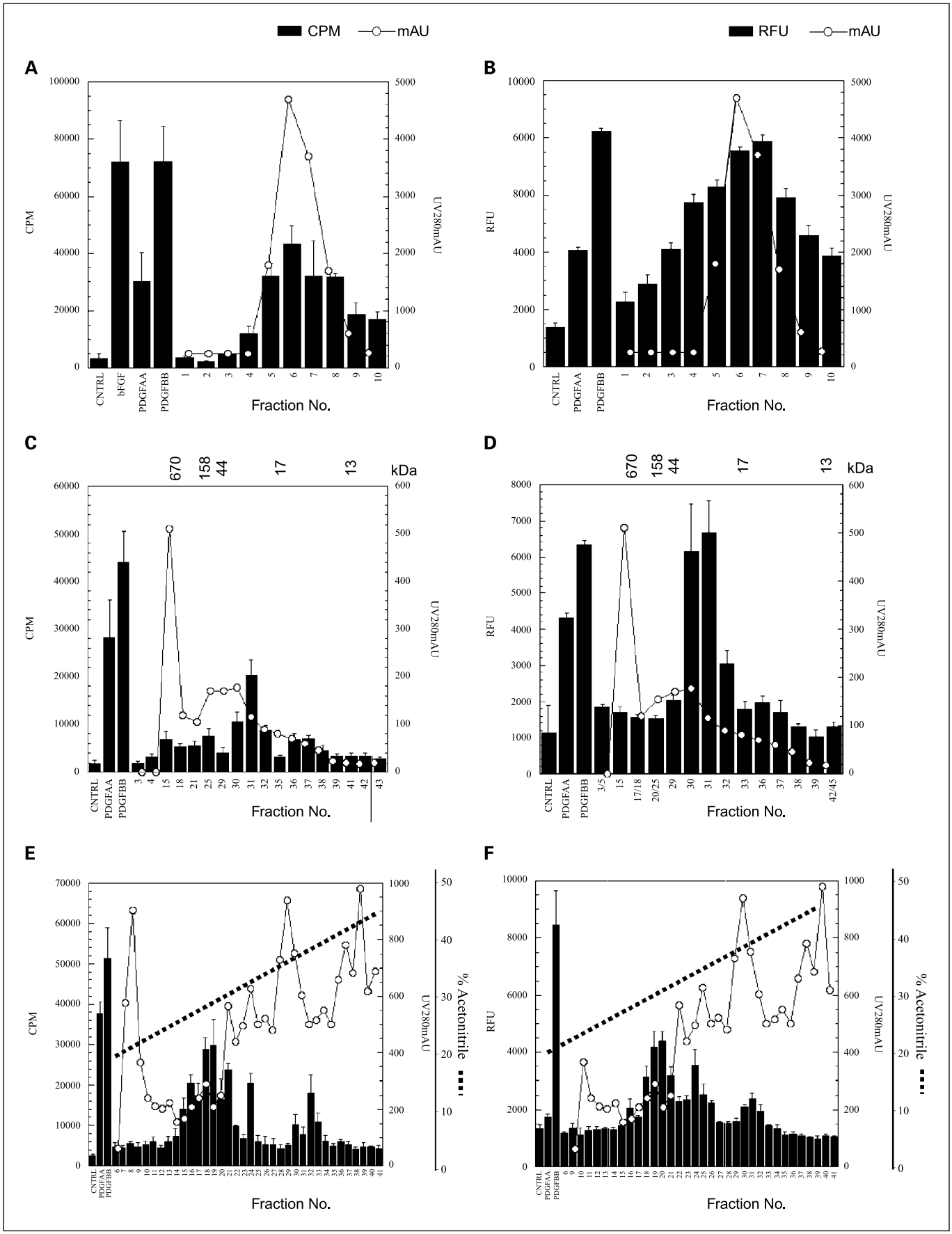

***PDGF/PDGFR signaling is critical to tumor growth* in vivo.** To discern whether the activities in the various fractions exerted their effects by signaling through PDGFRα or PDGFRβ, the size-excluded fractions were retested in the presence of neutralizing recombinant human PDGF receptors. Soluble PDGFRα, which primarily inhibits PDGFAA and PDGFCC signaling, abrogated the mitogenic (Fig. 4A) and chemotactic (Fig. 4B) activities detected in the size-excluded fractions. In contrast, the presence of soluble PDFGRβ, which primarily inhibits PDGFB and PDGFD signaling, did not affect either activity.

To further characterize the different bioactivities, we used of reverse-phase column chromatography. Once again, the prominent peak of mitogenic and chemotactic activity was found to coincide with the elution of PDGFAA (data not shown).

Given the significant levels of PDGFAA and PDGFCC expressed by the tumors and the effects of blocking PDGFRα signaling *in vitro*, we examined the effects of inhibiting PDGFRα signaling on tumor growth *in vivo*. A xenograft experiment was done, in which Calu-6 cells were injected s.c. into the rear flanks of immune-deficient mice. Beginning 24 hours later, the mice were treated i.t. with adenovirus encoding *LacZ* (Ad-LacZ), *Flt-IgG* (Ad-mFlt-IgG), or soluble forms of *PDGFRα* (Ad-PDFGRα-IgG) or *PDGFRβ* (Ad-PDGFRβ-IgG), and their effect on tumor growth was assessed. Compared with the Ad-LacZ-treated tumors, all of the treatments significantly affected the rate ($P < 0.01$; Fig. 4C) and the extent ($P < 0.001$; Fig. 4D) of tumor growth. Notably, Ad-PDGFRα treatment was as effective as treatment with Ad-mFlt-IgG (Fig. 4C and D). In representative histologic sections of treated tumors ($n = 6$ or 7 per group in each of two separate experiments), the areas of tumor necrosis, estimated visually, was similar in control Ad-LacZ-treated samples ($19 \pm 13\%$, $n = 12$) and Ad-PDGFRβ-treated samples ($23 \pm 14\%$, $n = 13$; P versus control = 0.47). In contrast, relative to Ad-LacZ controls, tumor necrosis was increased in Ad-Flt tumors ($36 \pm 26\%$, $n = 12$; $P = 0.055$ versus controls) and Ad-PDGFRα-treated tumors ($43 \pm 24\%$, $n = 12$; $P = 0.006$ versus controls). The extent of necrosis was not significantly different between Ad-Flt- and Ad-PDGFRα-treated groups ($P = 0.47$). We also tested the effects of the adenoviral constructs on the growth of established tumors. As single agents, the soluble PDGF receptors and mFlt-IgG effectively inhibited the growth of established tumors of an average size of ≈ 150 mm^3 (data not shown).

PDGFRα autocrine signaling has been described in gliomas and sarcomas but not in carcinomas (18, 38). However, it was important to show that the antitumor effects observed resulted from effects upon the host stromal cells rather than anti-proliferative effects on the tumor cells caused by disruption of an existing autocrine loop. Therefore, we tested the effects of the soluble PDGF receptors on Calu-6 proliferation *in vitro*. Calu-6 cell proliferation was unaffected by either receptor (Fig. 4E), even at levels 5-fold greater than those used to inhibit NIH3T3 fibroblast proliferation and migration (Fig. 4A and B). Additionally, Calu-6 cells failed to respond to several recombinant growth factors tested, including PDGFAA and BB; yet, they proliferated readily in complete medium (10% fetal bovine serum).

Expression of PDGFRα$^+$ is highest in fibroblasts in the tumor outer rim. To dissect the mechanisms underlying the antitumor effects observed, *in situ* hybridization analysis was done on Calu-6 tumor sections using probes for human and murine *PDGFA* and *PDGFB* and the murine *PDGFRα* and *PDGFRβ* (Fig. 5). As the adenoviral treatments did not affect host expression of any of the genes examined, only the Ad-LacZ-treated controls are provided. Human *PDGFA* is abundantly expressed throughout the tumor mass with particularly intense regions around areas of necrosis (Fig. 5A). In contrast, no signal was detected in the sense control. *PDGFB* was more weakly expressed throughout the tumor mass, with modest increases in intensity around necrotic regions. To assess the host's contribution of these factors, probes specific to murine *PDGFA* and *PDGFB* were used. *PDGFA* signal was weak and scattered throughout the tumor mass, whereas the *PDGFB* signal detected was associated with blood vessels (Fig. 5B). These results suggested that the majority of the PDGFA were produced by the tumor epithelium. To confirm these results, quantitative RT-PCR was done using primers that recognize both human and murine forms of *PDGFA*. When compared with the results obtained using primers specific for human *PDGFA* the results, normalized to *glyceraldehyde-3-phosphate dehydrogenase*, indicated that the preponderance of *PDGFA* in the tumors is produced by the tumor cells themselves and not host cells (data not shown). *In situ* hybridization revealed that the most intense expression of *PDGFRα* was localized to stromal fibroblasts at the tumor periphery (Fig. 5C). Alternatively, *PDGFRβ* displayed a punctuate pattern of expression, associated with discrete stromal cell clusters throughout the tumor. Because members of the PDGF family have been shown to affect the angiogenic process, there was a possibility that Ad-PDGFR-IgG treatment affected the expression of *VEGF*.

A *VEGF*-specific probe displays a modest signal from the fibroblasts within the stroma, with the highest intensity associated with the tumor cells at the periphery of the necrotic regions (Fig. 5D). The significant cross-reactivity of the probe for the human and murine *VEGF* transcripts made it difficult to discern any significant changes in *VEGF* expression resulting from the adenoviral treatments. Taqman analysis of tumor RNA using primers specific for murine *VEGF-A* indicated that treatment with Ad-PDGFRα resulted in an ~40% reduction in expression relative to Ad-LacZ (Supplementary Fig. S1).

Calu-6 tumors recruit PDGRFα$^+$ stromal fibroblasts. To verify these results, immunohistochemistry of the tumor samples was done using antibodies to murine PDGFRα, PDGFRβ, αSMA, and MECA-32, an endothelial PLVAP-specific antibody (Fig. 6). The most intense PDGFRα-specific staining localized to stromal fibroblasts present at the periphery of the tumor (Fig. 6B). Within the tumor mass, this stromal cell type seemed to exhibit

Fig. 2. Fractionation of Calu-6 conditioned medium. Column chromatography was used to enrich different bioactivities from Calu-6 conditioned medium. *A*, *C*, and *E*, fractions generated were assayed for mitogenic activity on NIH3T3 cells. CPM incorporated over fraction number. *B*, *D*, and *F*, fractions were also tested for chemotactic activity on NIH3T3 cells. Relative fluorescence units (*RFU*) over fraction number. Absorbance at 280 nm was monitored during chromatographic procedures. Protein molecular weight standards are presented as kDa. *A* and *B*, Calu-6 CM was subjected to cation-exchange chromatography, as described in the text. Fractions 4 to 8 (eluted with 1 mol/L NaCl) showed a peak of mitogenic and chemotactic activity. These fractions were pooled and further purified by size-exclusion chromatography. *C* and *D*, fractions 29 to 32 (apparent molecular weight = 20-45 kDa) contained a major peak of bioactivity that was pooled and subjected to C4-reverse-phase chromatography. *E* and *F*, fractions 15 to 22 contain a major peak of bioactivity. Columns, mean; bars, SE.

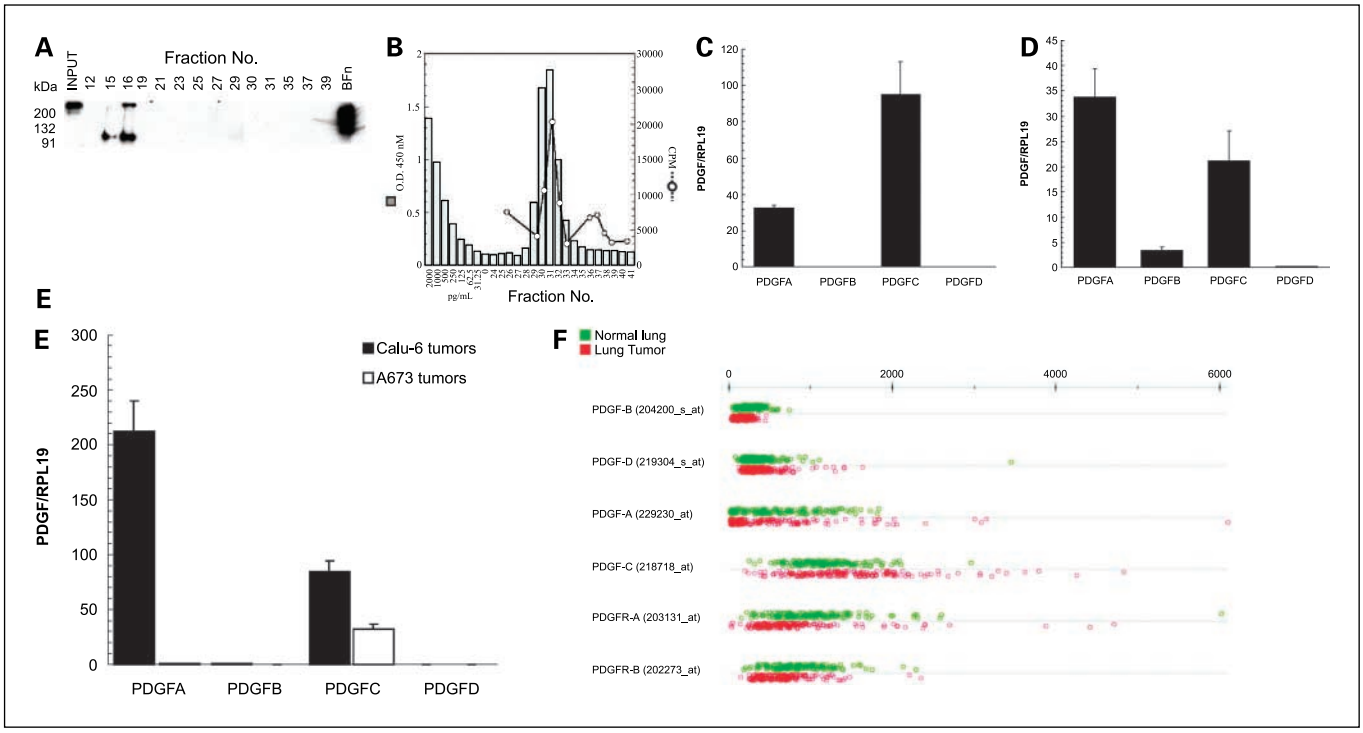

Fig. 3. PDGFAA is a major component of the bioactive fractions generated from Calu-6 conditioned medium. *A,* size-excluded fractions were concentrated 4-fold and analyzed, along with the INPUT (Calu-6 conditioned medium) and bovine fibronectin (*BFn*) controls, for the presence of fibronectin by Western blotting. *B,* size-excluded fractions represented in Fig. 2C and D were analyzed for the presence of PDGFAA (*solid gray columns*). The corresponding mitogenic activity is also given for each fraction in CPM. *C, D,* and *E,* quantitative RT-PCR analysis was used to examine the transcript levels of the PDGFA, PDGFB, PDGFC, and PDGFD chains in RNA isolated from Calu-6 (*C*) or HPAC (*D*) cells grown in monolayer as well as Calu-6–derived xenografted tumor RNA (*E*). The results were normalized to the levels obtained using probes specific for human ribosomal protein L19 (RPL19). From three experiments. Columns, mean; bars, SE. *F,* the signal intensity (arbitrary units) for each of the PDGFs in 138 normal lung samples and 159 lung tumor samples was computed using the Affymetrix MAS 5 software. Normal samples are shown in green above the respective lines for each PDGF, whereas tumor samples are shown in red; *t* statistics and their corresponding two-tailed *P*s were calculated using the R-program for statistical computing, assuming unequal variance in the normal and tumor groups.

a decreased expression of PDGFRα. In the surrounding tissue, expression of PDGFRβ localized predominantly to the vasculature (Fig. 6E). In addition, a low level of expression was associated with a portion of the fibroblast cells. Within the tumor mass, PDGFRβ expression also localized to blood vessels but was equivalently expressed in a major portion of the stromal fibroblasts. MECA-32 staining was done to more clearly identify blood vessels in the tumor periphery and in the tumor mass (Fig. 6C-E). Staining for αSMA in the normal stroma was strongly associated with vascular smooth muscle cells in a manner similar to the results of PDGFRβ staining (Fig. 6K). Within the tumor mass, αSMA expression remained vascular, but in addition, localized to nonvascular stromal cells in a pattern that was most consistent with that observed for PDGFRβ expression (Fig. 6L).

Discussion

In previous studies, Dong et al. showed a *VEGF*-null murine tumor's ability to overcome the need for VEGF by recruiting the host stroma, a significant contributor to tumor angiogenesis and growth, in a PDGFAA-dependent manner (29). Here, we show that this is also true of human tumor cells.

We initially focused on the response of Calu-6 tumors to treatment using an anti-human VEGF antibody mAb A4.6.1. These studies revealed a significant incorporation of host stromal cells, displaying the spindle-like fibroblast phenotype, into the Calu-6 tumor mass. The degree of stromal cell incorporation correlated strongly with the host-stromal contribution of VEGF and the ability of these tumors to resist treatment with mAb 4.6.1. In contrast, tumors without a substantial host-derived stromal component, such as the A673 rhabdomyosarcoma, are profoundly inhibited by mAb 4.6.1. These results suggest that recruitment of stromal fibroblasts might play an important role in tumor angiogenesis, by providing additional VEGF. Alternatively, recent studies indicate that tumor fibroblasts may contribute to angiogenesis through VEGF-independent pathways. Orimo et al. have reported that cancer-associated fibroblasts produce SDF-1, which in turn leads to recruitment of bone marrow–derived endothelial progenitor cells by the tumor vasculature (39). Thus, the elucidation of the mechanisms of tumor stroma recruitment is potentially important for our understanding of the development of resistance to anti-VEGF therapies.

Surprisingly, few studies have attempted to identify tumor-derived chemoattractants for stromal cells. Using conditioned medium from a colon carcinoma cell line, Morimoto et al. identified fibronectin fragments of 210 and 185 kDa as the major fibroblast chemoattractants (18). Similarly, other groups have identified fibronectin as a major fibroblast chemoattractant in lung injury and renal fibrosis models (17, 19, 40, 41). Although fibronectin was detected in the Calu-6 conditioned medium and size-excluded fractions, it was determined to represent a relatively minor portion of the chemotactic activity.

Table 3. PDGF expression in the conditioned media of various human tumor cell lines

Tumor cell line	PDGFAA (ng/mL)	PDGFBB (ng/mL)	Description	Tissue source
Calu-6	0.893	ND	Anaplastic carcinoma	Lung
HPAC	0.608	ND	Adenocarcinoma	Pancreas
CRL1739	0.364	ND	Gastic adenocarcinoma	Stomach
MDA231	0.374	ND	Breast adenocarcinoma	Breast
HT1080	0.335	ND	Fibrosarcoma	Connective tissue
SK-MES-1	0.326	ND	Squamous cell carcinoma	Lung; pleural effusion
NLSLIM-6	0.274	ND	Carcinoma	Colon
A673	0.062	ND	Rhabdomyosarcoma	Muscle

NOTE: Below the limits of detection of the ELISA (<31.2 pg/mL).
Abbreviation: ND, not detected.

In contrast, we detected significant levels of PDGFAA protein in the bioactive fractions generated from Calu-6 conditioned medium and, additionally, in the conditioned medium of a variety of cell lines whose tumors are associated with a significant stromal response *in vivo*. The absence of detectable levels of PDGFBB in these conditioned media was notable given that it is the most potent and tumorigenic of the PDGF family members (42, 43). Using quantitative RT-PCR and

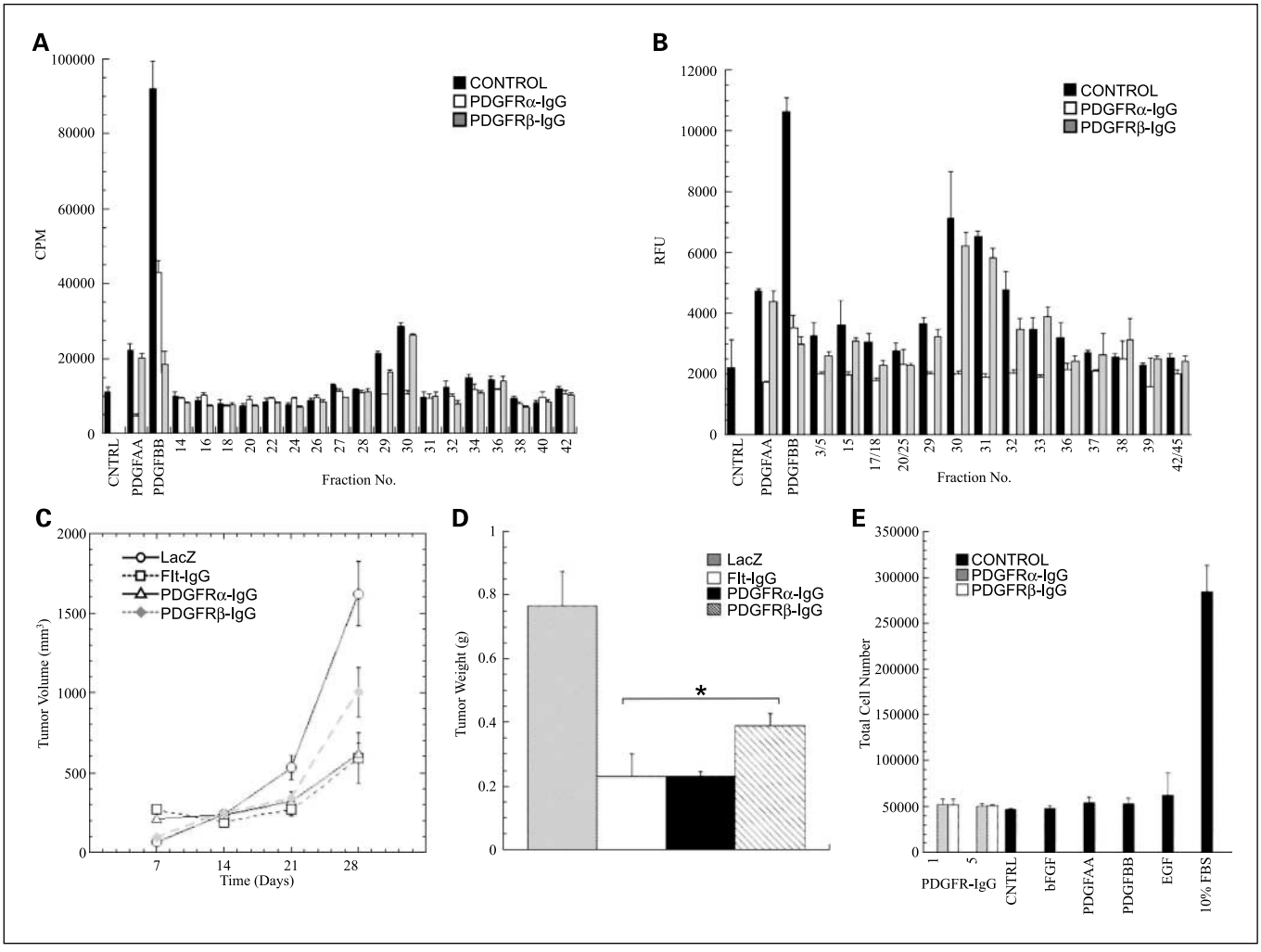

Fig. 4. Antagonizing PDGFR-signaling inhibits Calu-6 tumor growth *in vivo*. *A,* size-excluded fractions were tested for mitogenic activity alone and in the presence of recombinant soluble PDGFRα or PDGFRβ. *B,* in a similar manner, a migration assay was done with these fractions alone and in the presence of recombinant soluble PDGFRα or PDGFRβ. *C,* Calu-6 derived tumors were treated with adenovirus encoding β-galactosidase (LacZ), mFlt(1-3)-IgG, PDGFRα-IgG, or PDGFRβ-IgG. Tumor volume (mm^3) over time in days for each of the treatment groups. Columns, mean of six mice per group; bars, SE. Differences between groups were assessed by one-way ANOVA followed by a Tukey HSD pairwise analysis. $P < 0.001$ was considered significant. *D,* net weights of the Calu-6 tumors at the end of the experiment are presented as wet tumor weight (g) over adenoviral treatment. *E,* effects of soluble PDGFRα and PDGFRβ on the proliferation Calu-6 cell were examined *in vitro*. Total cell number over treatment.

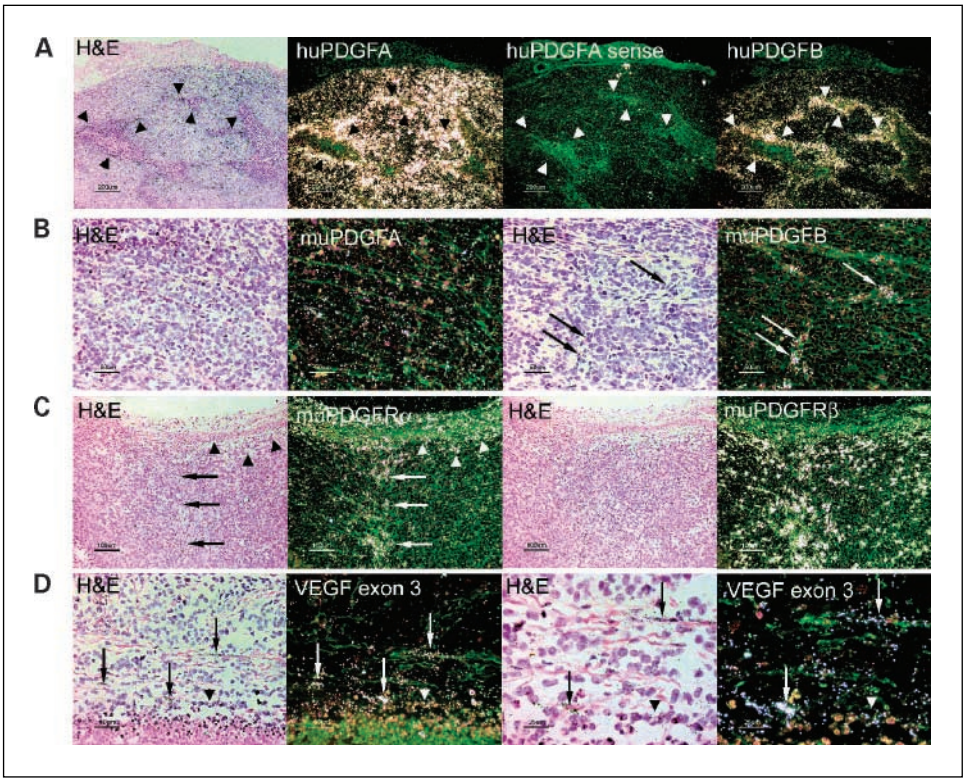

Fig. 5. *In situ* hybridization of Calu-6 tumors using *PDGFRα* and *PDGFRβ* probes. Paraffin sections of Ad-LacZ–treated Calu-6 tumors were hybridized with [^{33}P]-labeled riboprobes specific for human and murine *PDGFA* and *PDGFB* and murine *PDGFRα* and *PDGFRβ* as indicated. In all cases, control sense probe signal was found to be negligible. Only representative results are included. *A,* abundant expression human *PDGFA* is evident throughout the tumor mass, particularly around necrotic areas (*arrowheads*), whereas the sense control produces no signal. The human *PDGFB* signal is generally weak in the viable tumor with increased intensity around necrotic regions (*arrowheads*). *B,* murine *PDGFA* signal is weak and scattered throughout the tumor mass, whereas *PDGFB* signal occurs in discrete clusters consistent with vasculature (*arrows*). *C,* murine *PDGFRα* signal exhibits a stromal pattern with increased intensity at the tumor periphery (*arrowheads*) and in a region of infiltrating stromal cells (*arrows*). In contrast, *PDGFRβ* displays a more focal pattern of expression associated with discrete stromal cell clusters. *D,* a probe generated from exon 3 of the murine *VEGF* gene produces a modest signal in both the tumor (*arrowheads*) and stromal (*arrows*) compartments, whereas the control sense probe produced no signal. Parallel images were taken with dark-field or bright-field illumination. Bar, 200, 100, 50, or 25 μm, depending on magnification.

ELISA, we showed that Calu-6 tumors express significant levels of PDGFAA protein and *PDGFC* transcripts. In contrast, these tumors contained comparably lower levels of PDGFB. We showed that soluble PDGFRα but not PDGFRβ abrogates the chemotactic and mitogenic activities in the size-excluded fractions, supporting the presence of PDGFAA. However, given the lack of suitable antibody reagents, we are presently unable to confirm the presence of PDGFCC in either the Calu-6 conditioned medium or the Calu-6 tumors. To address the physiologic relevance of the results derived using the Calu-6 tumor model, we showed that tumors derived from a human pancreatic adenocarcinoma cell line also express significant levels of PDGFA and PDGFC. Similar to the Calu-6 tumors, these pancreatic tumors are characterized by their capacity to induce a significant stromal infiltration *in vivo* (37).

Interestingly, an earlier study (27) reported that PDGFA is important to initiate a desmoplastic response in a *ras*-transformed breast carcinoma cell line, in agreement with our findings in a lung carcinoma model. However, the functional significance of stromal recruitment was not explored in that study.

Studies done *in vitro* and *in vivo* have shown that, like PDGFA, PDGFC dimers signal primarily through PDGFRα to stimulate fibroblast proliferation, collagen deposition, and angiogenesis (44, 45). Our studies, along with those of others, have shown that PDGFC is expressed in a wide variety of tumor cell lines, indicating an active role for PDGFC in tumorigenesis (46). Coupled with the data showing that expression of PDGFC is significantly up-regulated in human lung tumors, our results implicate PDGFRα signaling in the development or progression of such types of solid tumors.

The high levels of PDGFA and PDGFC in the Calu-6 tumors prompted us to examine the effect of antagonizing the PDGFRα signaling pathway on tumor growth. Commonly used small-molecule receptor tyrosine kinase inhibitors of PDGF display characteristic nonspecific cross-reactivity with other receptor tyrosine kinases, making it difficult to distinguish the effects of targeting a single type of receptor on an individual class of cells from targeting several receptor classes on various different cell types (47). Therefore, we used adenovirus to maintain a sustained and robust expression of neutralizing forms of the PDGF receptors *in vivo*. We showed that disrupting PDGFRα signaling inhibits tumor growth as efficiently as blocking VEGF, and that this did not result from antiproliferative effects on the tumor cells themselves. This latter result was consistent with *in vivo* evidence showing the existence of PDGFRα autocrine signaling in gliomas and sarcomas but not in carcinomas (18, 38). The significant antitumor effects of adenoviral treatment prompted us try to identify the mechanism underlying these effects. The inhibitory effects of Ad-PDGFRβ are consistent with antivascular effects, such as inhibition of pericyte recruitment. Furthermore, the localization of PDGFRβ in fibroblasts within the tumor mass suggests that inhibition of stromal recruitment may also contribute to the effect.

In situ hybridization of tumor samples revealed particularly significant PDGFRα expression in the stromal fibroblasts at the periphery of the tumors, and this was confirmed by immunohistochemistry, which also indicated a lower level of PDGFRα expression in the cells that had become incorporated into the tumor. This localization of PDGFRα is intriguing, considering that several recent studies have emphasized that the tumor periphery is a particularly dynamic area. Tumor growth and resistance to vascular targeting agents are mediated by tumor cell proliferation starting at the outer rim (48). Furthermore, recruitment of bone marrow–derived endothelial progenitor

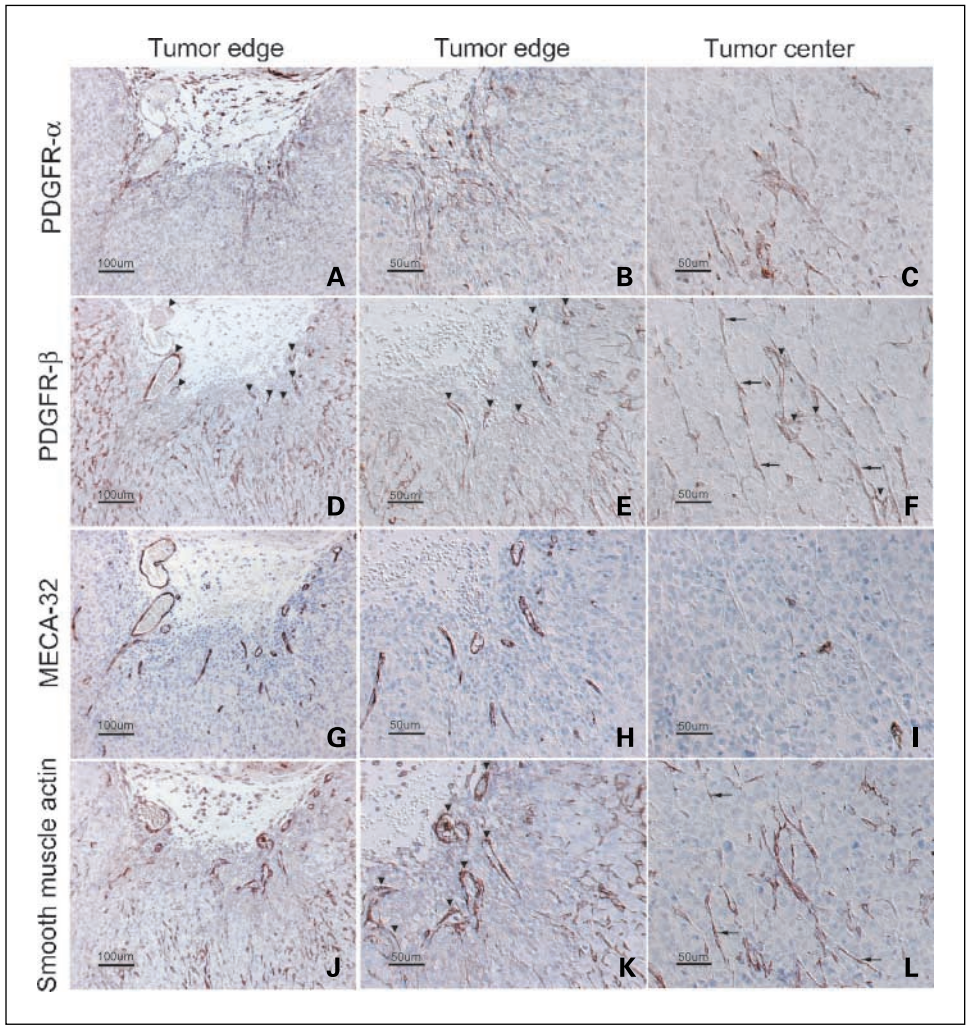

Fig. 6. Immunohistochemistry confirms that Calu-6 stromal fibroblasts express PDGFRα and PDGFRβ. Closely adjacent paraffin sections of Ad-LacZ-treated Calu-6 tumors were stained with antibodies to αSMA, PDGFRα, PDGFRβ, and PVLAP as indicated. *A* to *C,* murine PDGFRα expression localizes to cells with fibroblast morphology with highest intensity in the cells in the surrounding tissue (tumor edge, *A* and *B*). *D* to *F,* in the tumor periphery, PDGFRβ staining localizes predominantly to perivascular cells (*arrowheads*, compare *D-F* with *G-I*). Within the tumor mass, PDGFRβ displays a stromal staining pattern (*arrows*) and to a lesser extent associates with perivascular cells (*arrowheads*). *G* to *I,* MECA-32 murine PLVAP expression, localized to vascular endothelial cells, allowing correlation of vascular-specific PDGFR expression. *J* to *L,* within the tumor mass, αSMA displays a stromal pattern of expression consistent with fibroblasts (*arrows, L*), whereas its expression in the surrounding tissue is more vascular (*arrowheads, K*).

cells first occurs at the tumor periphery (49). Studies are ongoing to further characterize such PDGFRα-expressing cells.

The finding that Ad-PDGFRα administration resulted in a reduced expression of mVEGF is consistent with the view that decreased stromal-derived angiogenesis is, at least in part, responsible for the antitumor effects.

Studies in a variety of solid tumors have shown that the overexpression of PDGFAA and constitutively activated forms of PDGFRα are associated with a poor prognosis (50–52). Our results suggest that blocking the tumor-directed recruitment of PDGFRα$^+$ fibroblasts into the tumor mass underlies the significant antitumor effects observed in our xenograft experiments and may have implications for the treatment of these types of tumors. Our *in situ* hybridization and immunohistochemistry analyses revealed the appositional expression of PDGFB and PDGFRβ in the vasculature, consistent with a role for stromal cell paracrine signaling in pericyte recruitment and vessel maturation. This interaction has also been shown to be critical to tumor growth (53–55). Given the shown expression of PDGFRα and PDGFRβ by the stromal fibroblasts and pericytes, it is likely that the PDGF signaling pathways mediated by PDGFRα and PDGFRβ play distinct and complementary roles in the tumorigenic process.

Our studies highlight the critical role played by PDGFRα signaling and underscore the effect of targeting stromal fibroblasts, in addition to the endothelial cells and pericytes.

Acknowledgments

We thank Joe Kowalski for his helpful assistance, Kyu Hong and John Gutierrez for development of the murine VEGF ELISA, and Dr. Luc Desnoyer and Raji Kaul for the HPAC tumor samples used in these studies.

References

1. Folkman J. The role of angiogenesis in tumor growth. Semin Cancer Biol 1992;3:65–71.
2. Kataki A, Scheid P, Piet M, et al. Tumor infiltrating lymphocytes and macrophages have a potential dual role in lung cancer by supporting both host-defense and tumor progression. J Lab Clin Med 2003;140:320–8.
3. Desmouliere A, Guyot C, Gabbiani G. The stroma reaction myofibroblast: a key player in the control of tumor cell behavior. Int J Dev Biol 2004;48:509–17.
4. Bhowmick NA, Neilson EG, Moses HL. Stromal fibroblasts in cancer initiation and progression. Nature 2004;432:332–7.
5. Folkman J. Role of angiogenesis in tumor growth and metastasis. Semin Oncol 2002;29:15–8.
6. Lyden D, Hattori K, Dias S, et al. Impaired recruitment of bone-marrow-derived endothelial and hematopoietic precursor cells blocks tumor angiogenesis and growth. Nat Med 2001;7:1194–201.
7. Ferrara N. VEGF and the quest for tumour angiogenesis factors. Nat Rev Cancer 2002;2:795–803.
8. Ferrara N, Gerber HP, LeCouter J. The biology of VEGF and its receptors. Nat Med 2003;9:669–76.

9. Hurwitz H, Fehrenbacher L, Novotny W, et al. Bevacizumab plus irinotecan, fluorouracil and leucovorin for metastatic colorectal cancer. N Engl J Med 2004; 350:2335–42.

10. Grunstein J, Roberts WG, Mathieu-Costello O, Hanahan D, Johnson RS. Tumor-derived expression of vascular endothelial growth factor is a critical factor in tumor expansion and vascular function. Cancer Res 1999;59:1592–8.

11. Shi YP, Ferrara N. Oncogenic ras fails to restore an *in vivo* tumorigenic phenotype in embryonic stem cells lacking vascular endothelial growth factor (VEGF). Biochem Biophys Res Commun 1999;254:480–3.

12. Fukumura D, Xavier R, Sugiura T, et al. Tumor induction of VEGF promoter activity in stromal cells. Cell 1998;94:715–25.

13. Pilch H, Schlenger K, Steiner E, Brockerhoff P, Knapstein P, Vaupel P. Hypoxia-stimulated expression of angiogenic growth factors in cervical cancer cells and cervical cancer-derived fibroblasts. Int J Gynecol Cancer 2001;11:137–42.

14. Hoch RV, Soriano P. Roles of PDGF in animal development. Development 2003;130:4769–84.

15. Coltrera MD, Wang J, Porter PL, Gown AM. Expression of platelet-derived growth factor B-chain and the platelet-derived growth factor receptor beta subunit in human breast tissue and breast carcinoma. Cancer Res 1995;55:2703–8.

16. Kawai T, Hiroi S, Torikata C. Expression in lung carcinomas of platelet-derived growth factor and its receptors. Lab Invest 1997;77:431–6.

17. Sundberg C, Branting M, Gerdin B, Rubin K. Tumor cell and connective tissue cell interactions in human colorectal adenocarcinoma. Transfer of platelet-derived growth factor-AB/BB to stromal cells. Am J Pathol 1997;151:479–92.

18. Lokker NA, Sullivan CM, Hollenbach SJ, Israel MA, Giese NA. Platelet-derived growth factor (PDGF) autocrine signaling regulates survival and mitogenic pathways in glioblastoma cells: evidence that the novel PDGF-C and PDGF-D ligands may play a role in the development of brain tumors. Cancer Res 2002;62: 3729–35.

19. McGary EC, Weber K, Mills L, et al. Inhibition of platelet-derived growth factor-mediated proliferation of osteosarcoma cells by the novel tyrosine kinase inhibitor STI571. Clin Cancer Res 2002;8:3584–91.

20. Sjoblom T, Shimizu A, O'Brien KP, et al. Growth inhibition of dermatofibrosarcoma protuberans tumors by the platelet-derived growth factor receptor antagonist STI571 through induction of apoptosis. Cancer Res 2001;61:5778–83.

21. Beckmann MP, Betsholtz C, Heldin CH, et al. Comparison of biological properties and transforming potential of human PDGF-A and PDGF-B chains. Science 1988;241:1346–9.

22. Claffey KP, Abrams K, Shih SC, Brown LF, Mullen A, Keough M. Fibroblast growth factor 2 activation of stromal cell vascular endothelial growth factor expression and angiogenesis. Lab Invest 2001;81:61–75.

23. Skobe M, Fusenig NE. Tumorigenic conversion of immortal human keratinocytes through stromal cell activation. Proc Natl Acad Sci U S A 1998;95:1050–5.

24. Tuxhorn JA, McAlhany SJ, Yang F, Dang TD, Rowley DR. Inhibition of transforming growth factor-β activity decreases angiogenesis in a human prostate cancer-reactive stroma xenograft model. Cancer Res 2002; 62:6021–5.

25. Hu M, Pollock RE, Nicolson GL. Purification and characterization of human lung fibroblast motility-stimulating factor for human soft tissue sarcoma cells: identification as an NH_2-terminal fragment of human fibronectin. Cancer Res 1997;57:3577–84.

26. Morimoto M, Irimura T. Fibroblast migratory factor derived from mouse colon carcinoma cells: potential roles of fibronectin in tumor stroma formation. J Cell Biochem 2001;80:635–46.

27. Shoji S, Rickard KA, Ertl RF, Robbins RA, Linder J, Rennard SI. Bronchial epithelial cells produce lung fibroblast chemotactic factor: fibronectin. Am J Respir Cell Mol Biol 1989;1:13–20.

28. Shao Z-M, Nguyen M, Barsky SH. Human breast cancer desmoplasia is PDGF initiated. Oncogene 2000;19:4337–45.

29. Dong J, Grunstein J, Tejada M, et al. VEGF-null cells require PDGFR alpha signaling-mediated stromal fibroblast recruitment for tumorigenesis. EMBO J 2004;23:2800–10.

30. Kim KJ, Li B, Winer J, et al. Inhibition of vascular endothelial growth factor-induced angiogenesis suppresses tumour growth *in vivo*. Nature 1993;362: 841–4.

31. Tomayko MM, Reynolds CP. Determination of subcutaneous tumor size in athymic (nude) mice. Cancer Chemother Pharmacol 1989;24:148–54.

32. Balskovich MA, Li Q, Delarue FL, et al. Design of GFB-111, a platelet-derived growth factor binding molecule with antiangiogenic and anticancer activity against human tumors in mice. Nat Biotechnol 2000; 18:1065–70.

33. Holcomb IN, Kabakoff RC, Chan B, et al. FIZZ, a novel cysteine-rich secreted protein associated with pulmonary inflammation, defines a new gene family. EMBO J 2000;19:4046–55.

34. Lu LH, Gillette N. An optimized protocol for *in situ* hybridization using PCR-generated ^{33}P-labelled riboprobes. Cell Vision 1994;7:169–76.

35. Ferrara N, Chen H, Davis-Smyth T, et al. Vascular endothelial growth factor is essential for corpus luteum angiogenesis. Nat Med 1998;4:336–40.

36. Gerber HP, Kowalski J, Sherman D, et al. Complete inhibition of rhabdomyosarcoma xenograft growth and neovascularization requires blockade of both tumor and host vascular endothelial growth factor. Cancer Res 2000;60:6253–8.

37. Liang WC, Wu X, Peale FV, et al. Cross-species vascular endothelial growth factor (VEGF)-blocking antibodies completely inhibit the growth of human tumor xenografts and measure the contribution of stromal VEGF. J Biol Chem 2006;281:951–61.

38. Harsh GR, Keating MT, Escobedo JA, Williams LT. Platelet derived growth factor (PDGF) autocrine components in human tumor cell lines. J Neurooncol 1990; 8:1–12.

39. Orimo A, Gupta PB, Sgroi DC, et al. Stromal fibroblasts present in invasive human breast carcinomas promote tumor growth and angiogenesis through elevated SDF-1/CXCL12 secretion. Cell 2005;121:335–48.

40. Gharaee-Kermani M, Wiggins R, Wolber F, Goyal M, Phan SH. Fibronectin is the major fibroblast chemoattractant in rabbit anti-glomerular basement membrane disease. Am J Pathol 1996;148:961–7.

41. Kuwahara M, Kuwahara M, Bijwaard KE, Gersten DM, Diglio CA, Kagan E. Mesothelial cells produce a chemoattractant for lung fibroblasts: role of fibronectin. Am J Respir Cell Mol Biol 1991;5:256–64.

42. Guo P, Hu B, Gu W, et al. Platelet-derived growth factor-B enhances glioma angiogenesis by stimulating vascular endothelial growth factor expression in tumor endothelia and by promoting pericyte recruitment. Am J Pathol 2003;162:1083–93.

43. Sundberg C, Ljungstrom M, Lindmark G, Gerdin B, Rubin K. Microvascular pericytes express platelet-derived growth factor-β receptors in human healing wounds and colorectal adenocarcinoma. Am J Pathol 1993;143:1377–88.

44. Cao R, Brakenhielm E, Li X, et al. Angiogenesis stimulated by PDGF-CC, a novel member in the PDGF family, involves activation of PDGFR-alphaalpha and -alphabeta receptors. FASEB J 2002;16:1575–83.

45. Ponten A, Li X, Thoren P, et al. Transgenic overexpression of platelet-derived growth factor-C in the mouse heart induces cardiac fibrosis, hypertrophy, and dilated cardiomyopathy. Am J Pathol 2003;163: 673–82.

46. Uutela M, Lauren J, Bergsten E, et al. Chromosomal location, exon structure, and vascular expression patterns of the human PDGFC and PDGFC genes. Circulation 2001;103:2242–7.

47. Drevs J, Medinger M, Schmidt-Gersbach C, Weber R, Unger C. Receptor tyrosine kinases: the main targets for new anticancer therapy. Curr Drug Targets 2003;4:113–21.

48. Raben D, Ryan A. Vascular-targeting agents and radiation therapy in lung cancer: where do we stand in 2005? Clin Lung Cancer 2005;7:175–9.

49. Arbab AS, Pandit SD, Anderson SA, et al. MRI and confocal microscopy studies of magnetically labeled endothelial progenitor cells trafficking to sites of tumor angiogenesis. Stem Cells 2006;24:671–8.

50. Ebert M, Yokoyama M, Friess H, Kobrin MS, Buchler MW, Korc M. Induction of platelet-derived growth factor A and B chains and over-expression of their receptors in human pancreatic cancer. Int J Cancer 1995;62: 529–35.

51. Hirota S, Ohashi A, Nishida T, et al. Gain-of-function mutations of platelet-derived growth factor receptor α gene in gastrointestinal stromal tumors. Gastroenterology 2003;125:660–7.

52. Katano M, Nakamura M, Fujimoto K, Miyazaki K, Morisaki T. Prognostic value of platelet-derived growth factor-A (PDGF-A) in gastric carcinoma. Ann Surg 1998;227:365–71.

53. Abramsson A, Lindblom P, Betsholtz C. Endothelial and nonendothelial sources of PDGF-B regulate pericyte recruitment and influence vascular pattern formation in tumors. J Clin Invest 2003;112:1142–51.

54. Bergers G, Song S, Meyer-Morse N, Bergsland E, Hanahan D. Benefits of targeting both pericytes and endothelial cells in the tumor vasculature with kinase inhibitors. J Clin Invest 2003;111:1287–95.

55. Lindblom P, Gerhardt H, Liebner S, et al. Endothelial PDGF-B retention is required for proper investment of pericytes in the microvessel wall. Genes Dev 2003;17: 1835–40.